

# Effects of Powder Variation on the Microstructure and Tensile Strength of Ti6Al4V Parts Fabricated by Selective Laser Melting

Hengfeng Gu\*, Haijun Gong\*, J. J. S. Dilip\*, Deepankar Pal\*,  
Adam Hicks†, Heather Doak†, Brent Stucker\*

\*Department of Industrial Engineering,  
J. B. Speed School of Engineering, University of Louisville, Louisville, KY 40292  
†Mound Laser & Photonics Center, Dayton, OH

## Abstract

Metallic powders are used as raw materials in the Selective Laser Melting (SLM) process. These metal powders are typically available from more than one powder vendor. Even when powders have the same nominal chemical compositions, powders produced by different companies typically result in different powder particle size distributions and morphologies. These powder differences result in different powder bed thermophysical properties, which affect how the powder melts and solidifies. This paper studies the effect of powder variation on the microstructure and tensile strength of as-built SLM Ti6Al4V parts. Ti6Al4V powders from different vendors were used to fabricate parts via SLM. Powder characteristics, such as particle size distribution, morphology, and flowability, were obtained. Powder bed densities and thermal conductivities were measured and compared. The microstructures and tensile strengths were investigated by standard metallographic and tensile testing methods. Based on the experimental results, a correlation between the powder characteristics and part properties are discussed.

## Introduction

Selective laser melting (SLM) is a powder bed fusion based additive manufacturing process, which utilizes a laser beam as the energy source to scan and melt selected areas of metallic powders in order to fabricate a 3D part in a layer-by-layer fashion. The Ti-6Al-4V alloy is widely used in SLM for aerospace, automotive and biomedical applications due to its unique characteristics such as high strength to weight ratio, excellent corrosion resistance and wear performance [1,2,3].

Metal powders used in SLM are commercially available from different vendors. Due to different techniques and specifications used in powder manufacturing, different powder lots can have different properties even if they have the same chemical compositions. Such differences in powder properties may affect the powder bed thermophysical properties, which may later affect the as-built SLM part properties.

Liu *et al* investigated 316L stainless steel powders with 2 types of particle size distributions and the properties of as-built part using SLM, of which the results indicate that powders with different particle size distributions behave differently and thus cause a difference in an as-built part's quality [4]. Spierings *et al* found that a difference in the particle size distributions of 316L stainless steel powders from 2 different vendors affect as-built part density, surface quality and mechanical

properties [5]. Few studies have been done to investigate the relationship between the properties of powders, the powder bed and as-built parts in a comprehensive way.

This paper investigates the effect of Ti-6Al-4V powder variation on the powder bed thermophysical properties and the microstructure and tensile strength of as-built SLM parts. A model-guided processing parameter set is also applied in the SLM fabrication process to achieve nearly identical as-built part properties when Ti-6Al-4V powder properties vary.

## **Materials and experimental procedures**

### **Material selection and characterization**

Titanium pre-alloyed powders acquired from 3 different suppliers (EOS GmbH, LPW Inc. and Raymor Industries Inc.) were used in this study. The three types of powders with identical nominal chemical composition of 6wt% aluminum and 4wt% vanadium were manufactured using gas atomization. These 3 powder types were characterized according to their particle size distribution, morphology and flowability. Particle size distribution was captured using a particle analyzer (Microtrac S3000). The morphology of each type of powder was observed under a scanning electron microscope (FEI Nova Nano SEM). Angle of repose (AOR) was chosen as an indicator of powder flowability, which was obtained using a 3 inch diameter sectioned PVC pipe with a clear end film. The largest angles of the powder before it slipped during gentle counter-clockwise manual rotation of the pipe are shown in figure 1. Three replicates were done for each type of powder.

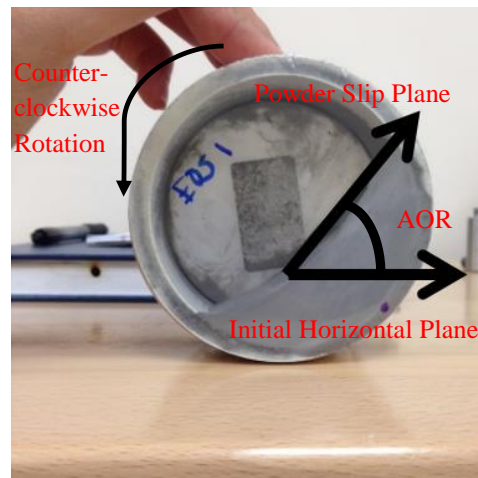


Figure 1 Angle of Repose (AOR) experimentation for EOS Ti6Al4V powder

## Powder bed characterization

Powder bed density and thermal conductivity are two factors which influence the Selective Laser Melting process since they may dramatically influence powder solidification and consolidation, thus impacting the quality of an as-built part. [4,6] Two simple preliminary experiments were designed and implemented in order to measure the values of these two factors for each type of Ti6Al4V powder bed.

A specially designed laser-milled stainless steel disk of 60mm diameter was used to measure the powder bed density of each type of Ti6Al4V powder. The disk was put on the build plate of the Direct Metal Laser Sintering Process Development Cell (DMLS PDC) at Mound Laser & Photonic Center, Inc (MLPC) and three layers of 0.03mm thick powders were spread over it for each measurement, which created a total 0.09mm height. The volume of the powder therefore could be determined. The disk was then removed from the platter and weighed both with and without powders, of which the difference is the mass of 3 layers of powders. The powder bed density was calculated using equation (1), where  $\rho_{Powder-bed}$  is the powder bed density,  $m_{Powder-bed}$  is the mass of powders on the disk, and  $V_{Powder-bed}$  is the volume of powders. 3 replicates were made for each powder type.

$$\rho_{Powder-bed} = \frac{m_{Powder-bed}}{V_{Powder-bed}} \quad (1)$$

In order to measure the powder bed thermal conductivity, a series of steady state thermal profiles were generated in the MLPC DMLS PDC using a range of fiber laser power intensities and a 125-250  $\mu\text{m}$  diameter laser beam so that the powder bed was gradually heated. The area covered by the illuminated laser is in the form of a circle with diameters of 1.25, 1.75 and 2.54 mm, where the hatch spacing between consecutive laser scans in the layer has been maintained at 100  $\mu\text{m}$  with a laser scan rate between 1000-5000mm/s to avoid powder melting. The processing parameters for powder bed thermal conductivity measurements are shown in table 1. The scan was continued for a minute in order for the powder bed to achieve a steady state thermal distribution. The schematic for the gradual laser heating scan pattern approximated using equation (2) is shown in figure 2, where  $R$  is the radius of the laser illuminated circle,  $h$  is the hatch spacing between consecutive laser scans and  $x$  is the x-axis coordinate for a specified spot within the laser illuminated circle and  $y$  is its y-axis coordinate. A FLIR camera was mounted beside the DMLS PDC for *in-situ* thermal profile recording, and the obtained thermal data were later analyzed for thermal conductivity calculations using the derived equation (3), where  $k$  is the calculated thermal conductivity value,  $A$  is the absorptivity of the powder,  $P$  is the laser power,  $\left(\frac{\rho_{powder-bed}}{\rho_{bulk}}\right)$  is the fraction density of the powder bed with respect to the Ti6Al4V bulk density,  $\alpha$  is the powder absorptivity rate,  $r$  is the distance between a specified spot in the laser illuminated circle and

geometrical center of the circle,  $R$  is the radius of the laser illuminated circle,  $\Delta T$  is the temperature difference between the steady state temperature at the specified spot with a distance of  $r$  to the geometrical center of the laser illuminated circle and room temperature, and  $v_x = \frac{2R}{T}$ , in which  $T$  is the time for finishing the illumination of the circle once (computed using a calculation of the approximate arc length divided by the scan speed =  $4 \frac{\sum_{i=1}^n (\sqrt{R^2 - (ih)^2})}{v}$  where  $i$  is number of intercepts on the x axis,  $h$  is hatch spacing and  $v$  is scan speed).

Table 1 Processing parameters of Ti6Al4V powder bed thermal conductivity measurement experiment

Parameters	Values
Beam diameter ( $\mu\text{m}$ )	125, 175, 250
Scan speed (mm/s)	1000, 2000, 3000, 4000, 5000
Hatch spacing ( $\mu\text{m}$ )	100
Laser power (W)	45, 68, 90
Scan circle diameter (mm)	1.25, 1.75, 2.54

$$y = \sqrt{(R^2 - x^2)} \sin\left(\frac{\pi x}{h}\right) \quad (2)$$

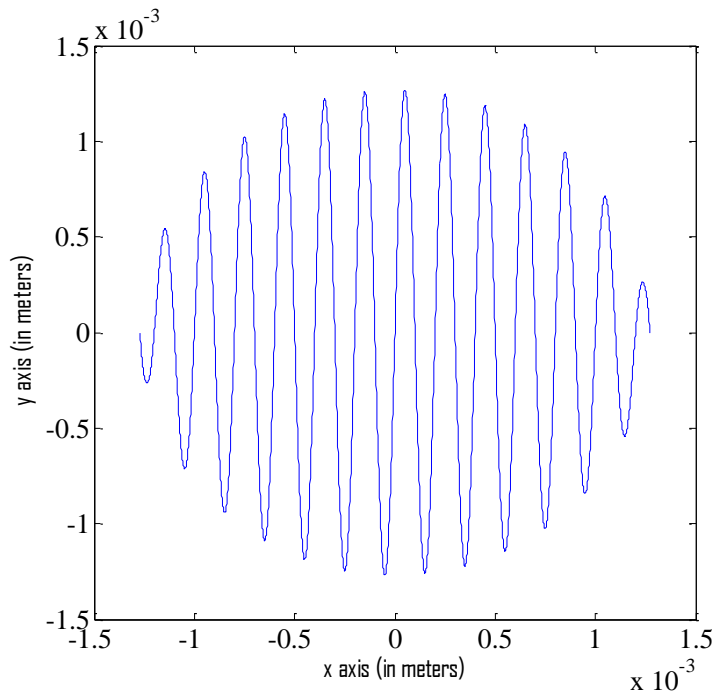


Figure 2 Schematic of the gradual laser heating scan pattern utilized for the measurement of Ti6Al4V powder bed thermal conductivity

$$k = AP \left( \frac{\rho_{\text{powder-bed}}}{\rho_{\text{bulk}}} \right) \left( \frac{1 - e^{-v_x \alpha r}}{4\pi r \Delta T R v_x \alpha} \right) \quad (3)$$

### Testing specimen fabrication process

Tensile testing specimens were designed according to ASTM E8/E8M-1. They were fabricated using EOS, LPW and Raymor Ti6Al4V powders respectively using an EOS DMLS M270 machine in argon purging atmosphere at the University of Louisville. An extra 5 mm was appended on both sides of the tensile testing specimen in the grip section for further microstructural analysis. Two sets of tensile testing specimens were fabricated as follows and 3 replicates of each parameter set were made:

#### Case A:

Specimens were fabricated using identical parameters for EOS, LPW and Raymor Ti6Al4V powders respectively in order to investigate the effect of powder variation on the as-built part quality under identical fabrication conditions. This parameter set was obtained by performing an empirically optimization of parameters for Raymor Ti6Al4V powders, as shown in table 2.

#### Case B:

EOS and LPW Ti6Al4V specimens were fabricated using model-guided processing parameter sets based on Case A by changing the hatch spacing values to keep a constant melt pool overlap for all 3 types of powders, as shown in table 3. The modified processing parameter sets were developed using novel finite element software developed at the University of Louisville [8]. The hatch spacing used in the machine was rounded up from the model predicted value to the next highest multiple of 10, as EOS software only accepts hatch spacing inputs as multiples of 10.

Table 2 Identical processing parameters for EOS, LPW and Raymor Ti6Al4V powders (Case A)

Laser Power (W)	Scan Speed (mm/s)	Layer Thickness ( $\mu\text{m}$ )	Hatch Spacing ( $\mu\text{m}$ )
186	1200	30	100

Table 3 Model-guided processing parameters for EOS and LPW Ti6Al4V powders based on Raymor empirically optimal parameter (Case B)

Supplier	Laser Power (W)	Scan Speed (mm/s)	Layer Thickness ( $\mu\text{m}$ )	Hatch Spacing ( $\mu\text{m}$ )
EOS	186	1200	30	80
LPW	186	1200	30	90
Raymor	186	1200	30	100

### Microstructural analysis

The extra grip section material was removed from the tensile testing specimen using a Buehler Isomet slow speed saw. These materials were further prepared using standard metallographic specimen preparation methods. Microstructures in YZ planes of 5 specimens were observed using an optical microscope (Olympus MX51).

### Tensile testing

The support structure was milled off the bottom surface of each tensile testing specimen, but all other surfaces were kept in their as-built condition. Tensile tests were carried out using an INSTRON system at the University of Louisville. An extensometer was used to record strain-stress data during the testing and 3 replicates were done for each processing parameter set.

## Results and Discussions

### Material characterization

#### (a) Particle size distribution

According to figure 3, EOS and LPW Ti6Al4V powder particles are uni-modally distributed within the range from  $20\mu\text{m}$  to  $50\mu\text{m}$ , while Raymor Ti6Al4V powder particles have a bi-modal distribution with a major particle size range from  $20\mu\text{m}$  to  $50\mu\text{m}$  and a minor particle size range from  $4\mu\text{m}$  to  $10\mu\text{m}$ . The mean volume diameter value (MV) and its corresponding standard deviation (SD) for the 3 types of powders are shown in figure 3.

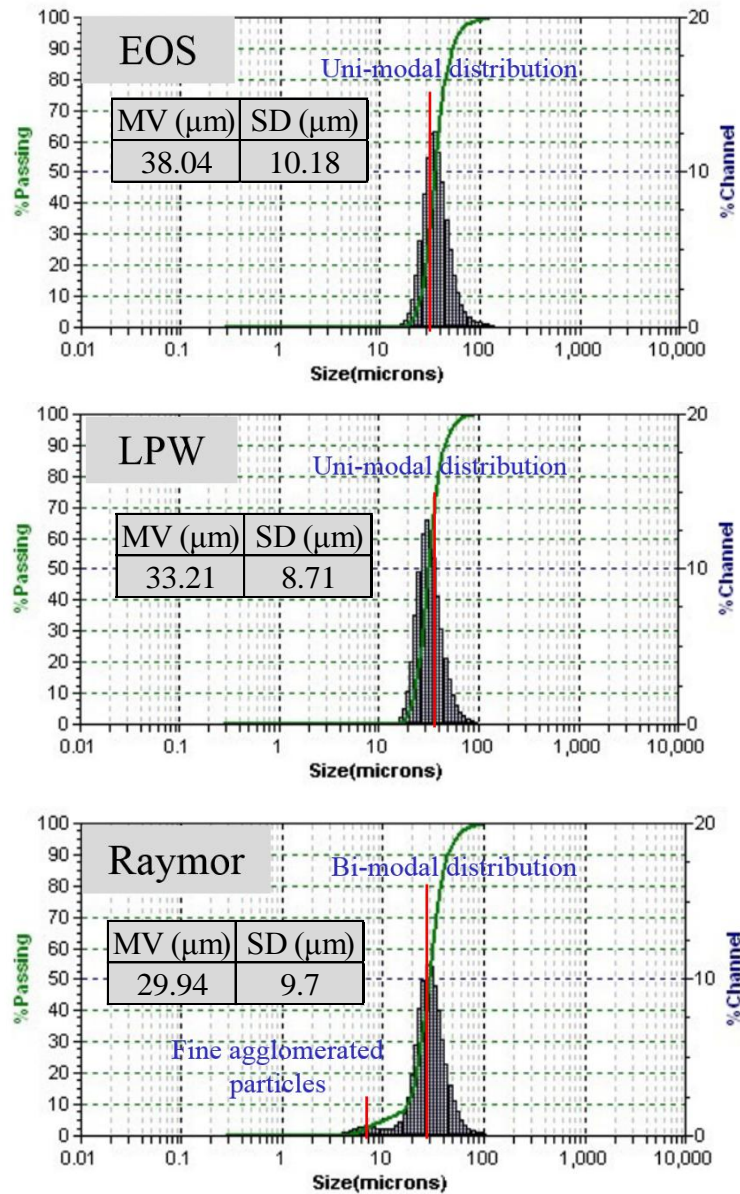


Figure 3 Particle size distribution graphs for EOS, LPW and Raymor Ti6Al4V powder particles

(b) Particle morphology

Figure 4 shows SEM images of EOS, LPW and Raymor Ti6Al4V powders. A majority of particles in all 3 types of powders appear spherical in shape. In particular, LPW powders seem to be more spherical compared to the other two types of powders, while a noticeable amount of particles with irregularly deformed shapes were found in EOS and Raymor powders according to the SEM images. In addition, there exists a significantly large amount of agglomerated fine particles in Raymor powders compared to EOS and LPW powders due to the bi-modal distribution in Raymor powder particles, which matches the PSA results.

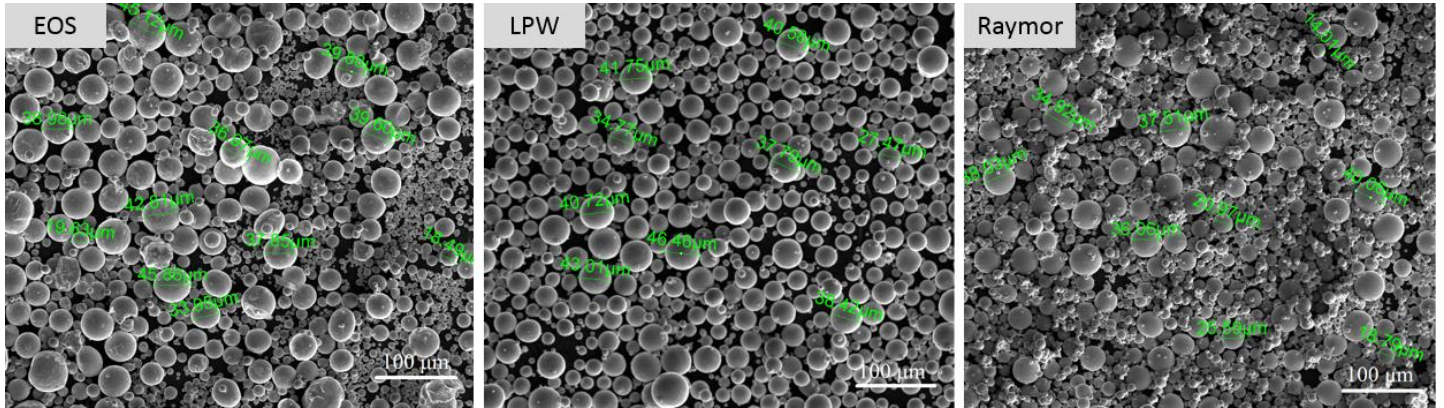


Figure 4 SEM images for EOS, LPW and Raymor Ti6Al4V powders

(c) Powder flowability

Angle of repose (AOR) is considered a good indicator of powder flowability; better powder flowability can be achieved at a smaller AOR value [7]. The comparison of AOR values for each type of powders is shown in figure 5, where a large difference of AOR values in 3 types of powders was found. The AOR value of Raymor powder is significantly higher than the other two types of powders, indicating that Raymor powder has the poorest flowability. This is probably due to the fine agglomerates within the powder, which increases inter-particle friction and reduces powder flowability. Meanwhile, AOR value for LPW powder is the lowest among the 3 types of powders, which may be explained by its noticeably more spherical particle shape found from the SEM images.

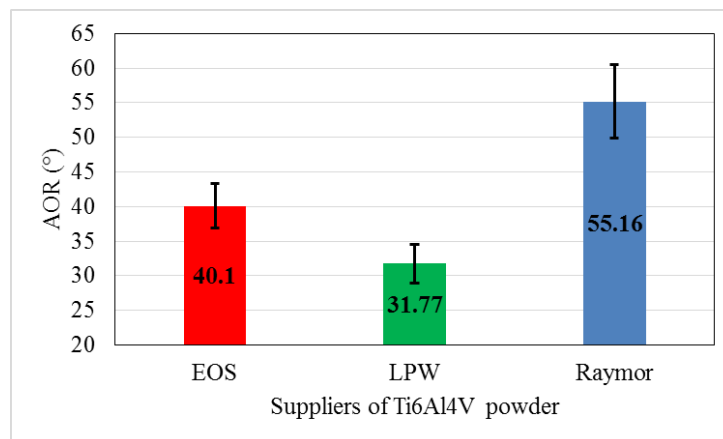


Figure 5 Angle of repose values for Ti6Al4V powders from 3 suppliers



## Powder bed characterization

### (a) Powder bed density

Figure 6 shows the comparison of Ti6Al4V powder bed density (PBD) values from 3 suppliers. There is no significant difference in PBD values for 3 types of powders; the PBDs of all 3 powders are approximately 47% of the Ti6Al4V bulk density of 4.42g/cc. The results indicates that powder flowability may not have a crucial impact on the powder bed density, even though it is reported to have an influence on the particle distribution in the powder bed [4].

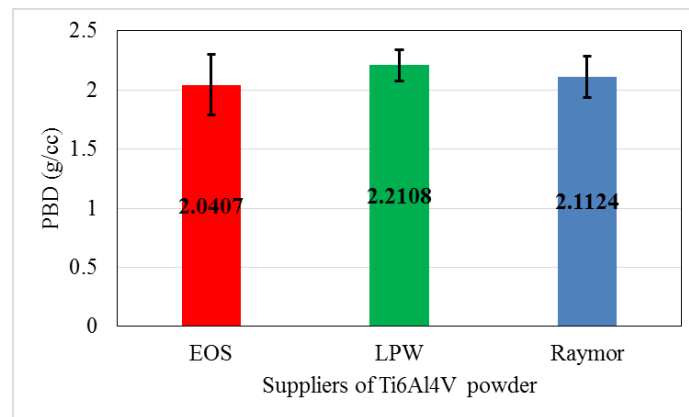


Figure 6 Ti6Al4V powder bed density from 3 suppliers

### (b) Powder bed thermal conductivity

Figure 7 shows the steady state thermal profiles of the powder beds for 3 types of Ti6Al4V powders in the laser illuminated areas. Raymor powder achieves much lower temperatures than EOS and LPW powder beds, indicating that the thermal properties of Raymor powder in the bed may be significantly different from EOS and LPW powder beds. One possible explanation can be that a lot of agglomerated fine particles within the Raymor powders may be easily sintered to the adjacent large powder particles at a relatively lower temperature, which may dramatically increase the overall thermal conductivity of the powder bed. The approximate percentage of the thermal conductivity for the powder bed compared to bulk Ti6Al4V properties were obtained using equation (3), and are shown in table 4. The trend of the calculated thermal conductivity values of 3 types of powders matches the above explanation.

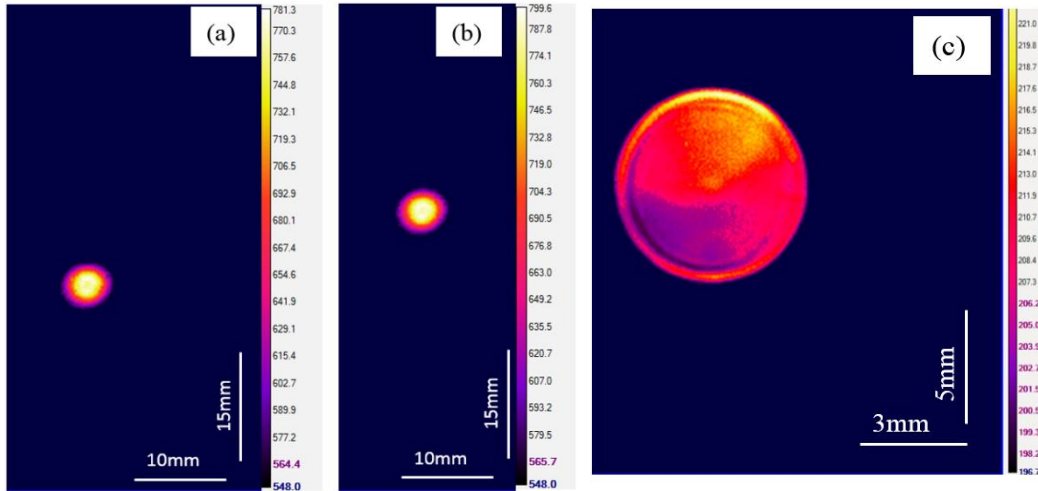


Figure 7 Steady state thermal profiles of (a) EOS, (b) LPW, and (c) Raymor Ti6Al4V powder bed using FLIR camera. (Images are not shown at the same scale.)

Table 4 Approximate percentage of thermal conductivity for the powder bed compared to bulk Ti6Al4V

Supplier	Approximate percentage of thermal conductivity of bulk Ti6Al4V (%)
EOS	~20
LPW	~20
Raymor	~60

### Microstructural analysis for as-built test specimens

Figure 8 shows the typical microstructures of specimens fabricated using the identical Raymor-based empirically optimal parameter set (Case A), where  $\alpha'$  martensite phases dominate the entire microstructure in all specimens. Due to the high cooling rate, all specimens experienced similar phase transformations during fabrication resulting in similar microstructures.  $\alpha'$  columnar grains with prior  $\beta$  grain boundaries grow in the build direction in the YZ plane. However, serious porosity occurs in specimens which were fabricated using EOS and LPW Ti6Al4V powders, while Raymor specimens achieve near full density under identical processing parameters. The difference in as-built part porosity is possibly linked to the disparity of the powder bed thermal properties during the fabrication process. When the same amount of laser energy is applied, more energy will be transmitted into the surrounding Raymor powder and thus form a wider melt pool and larger overlap than those formed using EOS and LPW powders due to the higher thermal conductivity in the Raymor powder bed. When adjacent melt pools do not overlap with each other, pores started to form in EOS and LPW specimens.

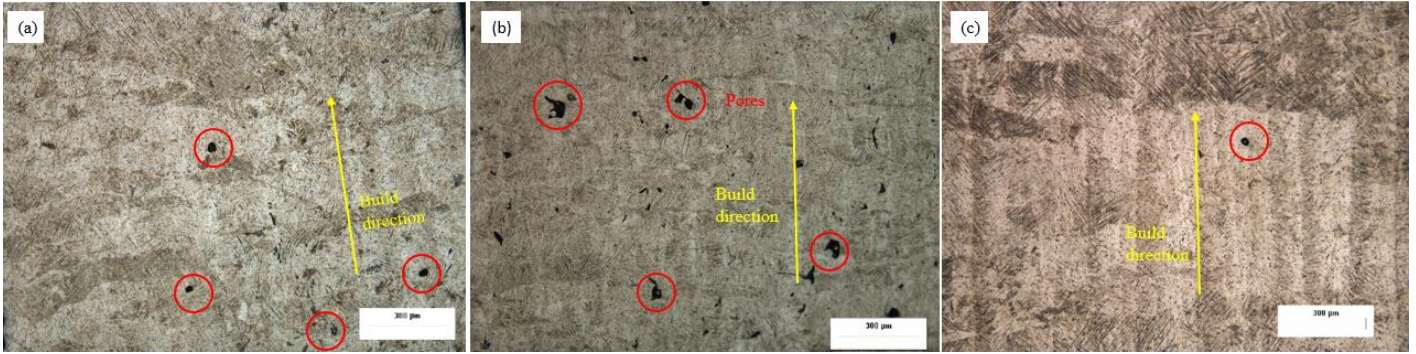


Figure 8 Microstructures in YZ plane of specimens fabricated using (a) EOS, (b) LPW, and (c) Raymor Ti6Al4V powders for identical Raymor-based empirically optimal parameters

The model-guided processing parameter sets for EOS and LPW powders (Case B) were applied during fabrication by only narrowing hatching spacing in order to achieve the same melt pool overlap as Raymor’s empirical optimal parameter set, thus seeking to avoid porosity in as-built EOS and LPW Ti6Al4V specimens. Comparison among microstructures of EOS, LPW and Raymor specimens fabricated using Case B are shown in figure 9, where all 3 specimens have reached near full density with the same phase composition as in figure 8.

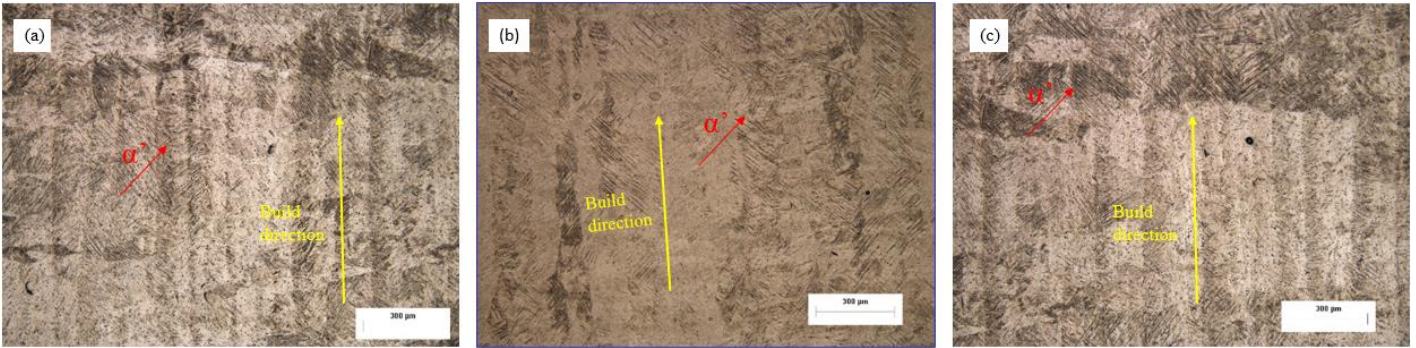


Figure 9 Microstructures in YZ plane of specimens fabricated using (a) EOS, (b) LPW, and (c) Raymor Ti6Al4V powders based on model-guided processing parameter sets

**Tensile testing**

Figure 10 shows the UTS and yield strength values for tensile specimens fabricated using Case A processing parameters. Both UTS and yield strength values for all 3 types of specimens were around the same level, which are approximately 1200MPa and 1100MPa respectively. The results indicate that the powder type variation does not have a significant influence on the as-built part’s tensile strength, even though it may dramatically affect the part’s fatigue performance due to the large difference in porosity.

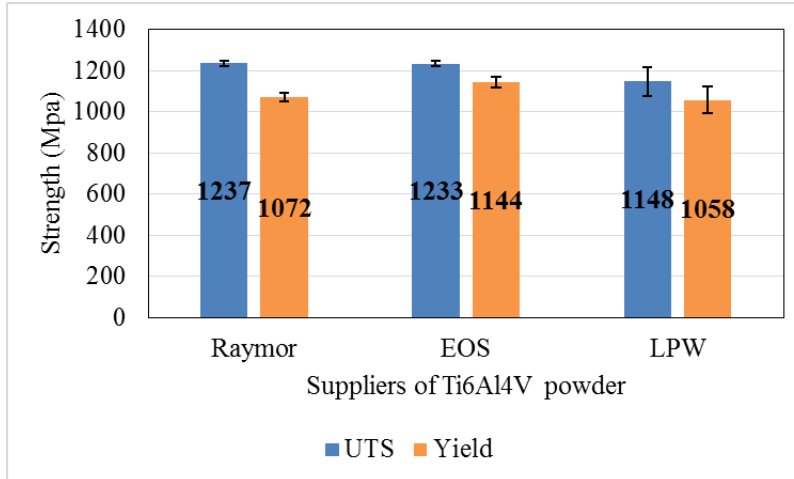


Figure 10 UTS and yield strength for parts fabricated using EOS, LPW and Raymor Ti6Al4V powders under Raymor-based empirically optimal processing parameters

Figure 11 shows the comparison of UTS and yield strength values for tensile testing specimens fabricated for Case B. Similarly to figure 10, no significant difference was found in UTS and yield strength values for parts manufactured using powders from 3 different suppliers. In addition, both UTS and yield strength values are at the same level as those in figure 10.

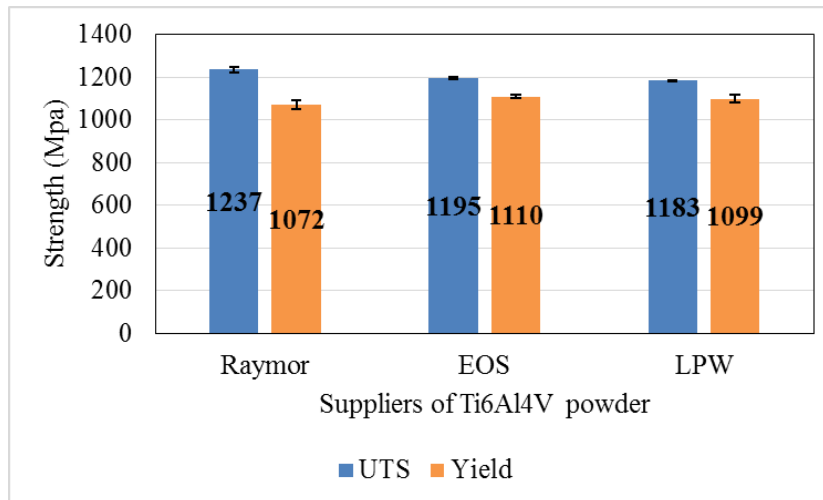


Figure 11 UTS and yield strength for parts fabricated using EOS, LPW and Raymor Ti6Al4V powders using model-guided processing parameter sets

### Summary

Ti-6Al-4V pre-alloyed powders obtained from 3 different suppliers were investigated in this study. Powder properties including particle size distribution, morphology, and flowability were characterized using various methodologies. All 3 types of powders appear spherical in shape,

however, a significantly large amount of fine particles were found in Raymor powders compared to the other two types of powders due to its bi-modal distribution. The flowability of Raymor powder is also much poorer than the other two powders caused by inter-particle friction introduced by these fine particles.

Powder bed densities of 3 types of Ti-6Al-4V powders were determined and no significant differences were found. However, the calculated Raymor powder bed thermal conductivity value was significantly higher compared to the values of the other two powder beds based on the powder bed thermal profiles captured using the thermal camera, which indicates that the thermal properties of Raymor powder may be completely different from the ones of the other two powders.

Tensile and metallurgical specimens were fabricated successfully under two sets of processing parameters; empirically optimal Raymor processing parameters for all 3 types of powders and model-guided processing parameters for each type of powder.

Serious porosity were found in EOS and LPW specimens using empirically optimal Raymor processing parameters, while the Raymor specimen was near fully dense. Specimens fabricated using all 3 types of powders under model-guided processing parameter sets achieved near full density. No significant difference in tensile strength were found in specimens fabricated using all 3 types of powders under all processing parameter sets.

Microstructures in all specimens appear very similar, where  $\alpha'$  columnar grains with prior  $\beta$  grain boundaries grow in the build direction in the YZ plane.

### **Future work**

The accuracy of the powder bed thermal conductivity method used in this study has not been determined. As it appears that powder bed thermal conductivity may be a significant factor for process parameter optimization, a well-established experimental for these types of experiments should be developed and its accuracy determined. Additionally, since there is no conclusive explanation for Raymor's significantly higher thermal conductivity value compared to the other two types of powders, further studies are needed to investigate the mechanism that leads to this large disparity.

No significant difference was found in tensile strength values between specimens with and without porosity, which was an unexpected outcome. More replicates are needed to make sure the validity of the effect of porosity on the as-built part tensile properties are valid.

### **Acknowledgement**

The authors thank the staff of the Rapid Prototyping Center at the University of Louisville and Mound Laser & Photonics Center, Inc for their help. We gratefully acknowledge the support of the Air Force Research Laboratory through contract FA8650-13-M-5060.

## References

- [1] Antonysamy, A. A. (2012). Microstructure, texture and mechanical property evolution during additive manufacturing of Ti6Al4V alloy for aerospace applications.
- [2] Atar, E., Kayali, E. S., & Cimenoglu, H. (2008). Characteristics and wear performance of borided Ti6Al4V alloy. *Surface and Coatings technology*, 202(19), 4583-4590.
- [3] Murr, L. E., Quinones, S. A., Gaytan, S. M., Lopez, M. I., Rodela, A., Martinez, E. Y., ... & Wicker, R. B. (2009). Microstructure and mechanical behavior of Ti-6Al-4V produced by rapid-layer manufacturing, for biomedical applications. *Journal of the mechanical behavior of biomedical materials*, 2(1), 20-32. Liu, B., Wildman, R., Tuck, C., Ashcroft, I., & Hague, R. (2011).
- [4] Liu, B., Wildman, R., Tuck, C., Ashcroft, I., & Hague, R. (2011). Investigation the effect of particle size distribution on processing parameters optimisation in Selective Laser Melting process. *Additive Manufacturing Research Group, Loughborough University*.
- [5] Spierings, A. B., Herres, N., & Levy, G. (2011). Influence of the particle size distribution on surface quality and mechanical properties in AM steel parts. *Rapid Prototyping Journal*, 17(3), 195-202.
- [6] Zhu, H. H., Fuh, J. Y. H., & Lu, L. (2007). The influence of powder apparent density on the density in direct laser-sintered metallic parts. *International Journal of Machine Tools and Manufacture*, 47(2), 294-298.
- [7] Geldart, D., Abdullah, E. C., Hassanpour, A., Nwoke, L. C., & Wouters, I. (2006). Characterization of powder flowability using measurement of angle of repose. *China Particuology*, 4(3), 104-107.
- [8] Pal, D., Patil, N., Nikoukar, M., Zeng, K., Haludeen, K.R., and Stucker, B.E. (2014). An Integrated Approach to Cyber-Enabled Additive Manufacturing using Physics based, Coupled Multi-scale Process Modeling. *Journal of Manufacturing Science and Engineering*, (invited for special series on Additive Manufacturing), accepted for publication.